arXiv:1403.5165v1 [cond-mat.mes-hall] 20 Mar 2014

Optomechanical coupling between a graphene mechanical resonator and a superconducting microwave cavity

V. Singh, S. J. Bosman, B. H. Schneider,

Y. M. Blanter, A. Castellanos-Gomez and G. A. Steele*

Kavli Institute of NanoScience, Delft University of Technology,

PO Box 5046, 2600 GA, Delft, The Netherlands.

(Dated: March 21, 2014)

Abstract

The combination of low mass density, high frequency, and high quality-factor make graphene mechanical resonators[1–8] very attractive for applications such as force sensing, mass sensing, and exploring the quantum regime of mechanical motion. Microwave optomechanics with superconducting cavities[9–14] offers exquisite position sensitivity[10] and enables the preparation and detection of mechanical systems in the quantum ground state[15,16]. Here, we demonstrate for the first time coupling between a graphene resonator and a high-Q superconducting cavity. We achieve a displacement sensitivity of 55 fm/$\sqrt{\text{Hz}}$ and measure mechanical quality factors up to 220,000, both significantly better than shown before for graphene. Optomechanical coupling is demonstrated by optomechanically induced reflection (OMIR) and absorption (OMIA) of microwave photons[17–19]. We observe 17 dB of mechanical microwave amplification[13] and the onset of normal mode splitting[12,20], both signatures of strong optomechanical backaction. We extract the cooperativity C, a characterization of coupling strength, quantitatively from the measurement with no free parameters and find $C = 8$, promising for the quantum regime of graphene motion.

After the initial demonstration of graphene mechanical resonators[1–3], there has been a considerable progress in harnessing the unique mechanical properties of graphene for mass sensing[2], studying nonlinear mechanics[5,6], and voltage tunable oscillators[7,8]. Graphene is also potentially attractive for experiments with quantum motion: the high quality factor[4,5] and low mass density of graphene resonators result in large zero point fluctuations in a small bandwidth. The high frequency of graphene resonators also provides low phonon occupation at cryogenic temperatures. Previously employed optical[1] and radio frequency (RF) techniques[2,3,5,6] enabled detection and characterization of graphene resonators, but achieved limited displacement sensitivity with an unclear path towards the quantum regime.

A possible route to the ultimate limit in sensitivity is cavity optomechanics[21]. A natural candidate for implementing cavity optomechanics with graphene resonators is a high-Q superconducting microwave cavity, capable of detecting motion near and below the standard quantum limit[10,11]. Cavity optomechanics has also been used to bring mechanical systems into their quantum ground state with sideband cooling[15,22] and to entangle microwave photons with the motion of a mechanical resonator[16]. Combining graphene with superconducting cavities in such a way that both retain their excellent properties, such as their high quality factors, is technologically challenging.

Here, we present a graphene mechanical resonator coupled to a superconducting cavity. Using a deterministic all-dry transfer technique[23] and a novel microwave coupling design, we are able to combine these two without sacrificing the exceptional intrinsic properties of either. Figures 1(a) and (b) show optical and electron microscope images of the device. The superconducting cavity is a quarter wavelength coplanar waveguide (CPW) resonator. Microwave photons are coupled in and out of the cavity via a feedline that is capacitively coupled to the CPW center conductor by a gap capacitor. This gap capacitor also includes a small gate electrode that extends from the feedline into the CPW center conductor (Figure 1(b)). The gate is thinned down in a second etch step so that it is 150 nm below the surface of the CPW center conductor metal. In the last step of fabrication, a multi-layer graphene flake (thickness $\sim$ 10 nm) is transferred over the hole, forming a capacitor between the superconducting CPW resonator and the feedline. Figure 1(b) shows a false color tilted angle scanning electron microscope image of the device measured here, consisting of a graphene drum of 4 μm in diameter suspended above the gate electrode.

An effective circuit model of the superconducting cavity (SC) with the embedded graphene resonator is shown in Figure 1(c). The cavity can be modeled by an effective lumped element capacitance C_{sc} and inductance L_{sc}. In addition, there are two extra capacitances to the microwave feedline, one from the graphene drum C_g and one from the fixed coupling capacitor C_c. The motion of graphene dispersively modulates the cavity frequency ω_c through the change in C_g : $\omega_c(x) = 1/\sqrt{L_{sc}(C_{sc} + C_c + C_g(x))}$ [24]. The use of the feedline capacitance to couple to the graphene resonator has some convenient practical advantages. In particular DC gate voltages (for tuning the mechanical frequency) and low frequency RF voltages (for electrostatically driving the mechanical resonator) can easily be applied to the microwave feedline without spoiling the quality factor of the superconducting cavity.

Figure 1(d) shows the measured reflection coefficient ($|S_{11}|$) of the cavity at $T = 14$ mK. A fit to the data yields a resonant frequency $\omega_c \approx 2\pi \times 5.9006$ GHz, external dissipation rate of $\kappa_e = 2\pi\times188$ kHz and a total dissipation rate of $\kappa = 2\pi\times242$ kHz. The coupling efficiency $\eta = \kappa_e/\kappa \approx 0.77$ ($> 1/2$) indicates that the cavity is overcoupled. (See supplementary information (SI) for additional cavity characterization). Based on the designed impedance of the cavity ($Z_0 = 50\ \Omega$) and geometric capacitance of graphene resonator $C_g \approx 670$ aF, we estimate the cavity pull-in parameter to be $G = \frac{d\omega_c}{dx} \approx 2\pi \times 31$ kHz/nm.

In Figure 2, we characterize the mechanical properties of the graphene resonator. To probe the resonant dynamics of the graphene resonator, we have used a homodyne measurement scheme[9]. Here, the cavity is used as an interferometer while injecting a microwave signal near ω_c. To drive the graphene mechanical resonator, we add a small RF signal (V_{ac}) and a DC voltage (V_g) to the microwave feedline. The oscillating motion of the graphene resonator modulates the power reflected by the cavity, which is used to read out the mechanical motion (see SI for detailed setup). Figure 2(a) shows the mechanical response of graphene resonator. A Lorentzian lineshape fit yields a mechanical resonant frequency $\omega_m \approx 2\pi\times36.233$ MHz and the mechanical quality factor of $Q_m \approx 159{,}000$. The resonance frequency ω_m is much larger than the cavity linewidth κ, placing us in the sideband resolved limit, a prerequisite for sideband cooling. Using the cavity as an interferometer, we achieve a displacement sensitivity of 55 fm/$\sqrt{\text{Hz}}$, significantly better than reported in previous graphene experiments[6,7].

Using a DC voltage applied to the gate electrode, we can also tune the frequency of the graphene resonator. Figure 2(b) shows the colorscale plot of the demodulated homodyne

signal measured while sweeping the mechanical drive frequency and the gate voltage. The resonance frequency ω_m decreases for non-zero gate voltage. Such a behavior has been observed before for graphene resonators and is due to electrostatic softening of the spring constant[3]. We also find that the quality factor of the graphene resonator is gate voltage dependent (see SI for detailed measurement). As the electromechanical driving force ($F_{ac} = \frac{dC_g}{dx} V_{ac} V_g$) vanishes at zero gate voltage, the measured signal disappears near $V_g = 0$ V.

In Figure 3, we demonstrate optomechanical coupling between the graphene mechanical resonator and the cavity, mediated by radiation pressure forces. Figure 3 shows measurement of the cavity similar to Figure 1(d), but now in presence of a strong drive signal that is detuned from the cavity frequency. The frequency is chosen such that $\omega_d = \omega_c + \omega_m$ ($\omega_c - \omega_m$), referred as driving the blue (red) detuned mechanical sideband. Including this second detuned drive tone, the cavity response acquires a sharp peak (Figure 3(a) for the blue sideband) or a sharp dip (Figure 3(b) for the red sideband) centered at the cavity resonance frequency. The sharp peak in Figure 3(a) when driving on the blue sideband corresponds to optomechanically induced reflection (OMIR) of microwave photons, the same phenomenon as optomechanically induced transparency (OMIT)[17–19], but now in a reflection geometry. In OMIT, an analogue of electromagnetically induced transparency (EIT) in atomic physics, a transparency window opens in the absorption resonance of the cavity due to the optomechanical coupling to the mechanical resonator. Driving on the red sideband, Figure 3(b), the cavity shows a sharp dip in the reflectivity of the cavity, corresponding to a process of optomechanically induced absorption (OMIA)[14].

Qualitatively, reflection and absorption features in the cavity response can be understood as follows. Consider the case of blue detuned driving shown by the schematic in Figure 3(a). Under the influence of a strong sideband drive signal (ω_d, blue arrow) and a weak probe signal (ω_p near ω_c, black arrow), the beat between the two microwave signals generates a radiation pressure force that oscillates at $\Omega \approx \omega_m$ (green arrow), schematically shown by process 1. This oscillating radiation force at frequency Ω coherently drives the graphene resonator. Mechanical motion of the graphene resonator in turn modulates the drive field resulting in a field appearing at $\omega_d + \Omega$ ($= \omega_p$, pink arrow) schematically shown by process 2. Being a coherent process, the upconverted field appearing at ω_p has a definite phase relation with the probe field. Depending on the phase difference, these fields at ω_p can either interfere constructively or destructively to produce an OMIR or OMIA features in

the cavity response. In contrast to the first observation of the OMIT[18], here we observe OMIR on the blue sideband instead of the red sideband. This is a consequence of the overcoupled cavity ($\eta > 0.5$) studied here (see SI for details).

In the context of characterizing the graphene resonator, the radiation pressure driving force allows us to measure Q_m at $V_g = 0$ V, which is inaccessible in the homodyne measurement scheme with electrostatic driving. Using OMIA, we find quality factors as high as $Q_m \approx 220{,}000$ at zero gate voltage, highest quality factor detected for a graphene resonator (additional data in the SI). Furthermore, inside the OMIA window, a fast change in the phase response of the microwave signal can result in a long group delay of microwave photons[19,25]. This delay can be used to implement a microwave photon storage device using a mechanical resonator (additional data in the SI). For our device, we estimated a storage time of 10 ms, comparable in magnitude to that recently demonstrated in conventional mechanical resonators[25] and equivalent to the delay from a hundreds of kilometers long coaxial cable.

In Figure 4, we explore the optomechanical interaction with the graphene resonator for larger coupling strengths. The optomechanical coupling strength (g) is tunable by the number of drive photons inside the cavity (n_d) as $g = Gx_{zpf}\sqrt{n_d} = g_0\sqrt{n_d}$, where x_{zpf} is the amplitude of quantum zero point fluctuations of the mechanical resonator and g_0 is the single photon coupling strength[21]. Figure 4(a) shows the cavity response while driving at the blue sideband with $n_d \approx 10^8$. Compared to the reflection feature show in Figure 3(a), we see that the OMIR peak has increased such that the reflection coefficient now exceeds unity, indicating more probe photons are coming out than we are putting in. This gain of microwave photons arises from mechanical microwave amplification[13] by the graphene resonator. We are able to achieve up to ∼17 dB gain with a number of added photons noise that can theoretically be as low as the number of thermal phonons (n_{th}) in the mechanical resonator[13] (at $T = 14$ mK, we expect $n_{th} \approx 8$). The origin of microwave amplification can also be understood in terms of the optomechanical backaction on the cavity: when the coupling strength becomes sufficiently strong such that $4g^2/\gamma_m$ overcomes internal dissipation rate of the cavity κ_i, the net effective internal damping rate of the microwave cavity becomes negative.

Figure 4(b) shows the cavity response for a red detuned drive with $n_d \approx 5 \times 10^8$. In contrast to Figure 3(b), we see that the absorption feature has become a reflection (trans-

parency) window. This crossover occurs when the optomechanical coupling becomes sufficiently strong such that effective internal dissipation rate of the cavity $\kappa_i^{eff} = \kappa_i + \frac{4g^2}{\gamma_m}$ exceeds the external dissipation rate κ_e. The data in Figure 4(b) shows clearly that we have passed this point. Also, the reflection window in Figure 4(b) is considerably larger in width than in Figure 3(a). This is an indication of optomechanical backaction on the graphene resonator. Similar to the modification of the internal dissipation rate of the cavity, the mechanical dissipation rate (γ_m) is also modified, $\gamma_m^{eff} = \gamma_m \left(1 + \frac{4g^2}{\kappa\gamma_m}\right)$, leading to the broadening of the OMIR feature and onset of the normal mode splitting of the cavity resonance[12,26]. This can also be seen clearly from the avoided crossing in the cavity response when detuned drive is swept across the red sideband as shown in Figure 4(c).

A useful feature of OMIA-OMIR data is that height of the peak or depth of the dip allows one to extract $\frac{4g^2}{\kappa\gamma_m} \equiv C$, the optomechanical cooperativity, with no free parameters. The cooperativity C is an important figure of merit for optomechanical experiments. For example, in sideband resolved limit, an important criteria for cooling the mechanical resonator to its quantum ground state is $C + 1 > \bar{n}_{th}$, where $\bar{n}_{th}$ is the number of thermally excited quanta in the resonator[21]. Figure 4(d) shows the cooperativity of our device extracted from the OMIA data as a function of the number of red detuned drive photons inside the cavity (n_d). Increasing n_d, we have been able to achieve $C = 8$. The horizontal error bar in the data results from the uncertainty in determining the power reaching the sample. Although C should scale with n_d, in our device the intrinsic mechanical quality factor begins to decrease at higher cavity power leading to deviation from a straight line fit. For low number of drive photons, the slope of line $\frac{dC}{dn_d} = \frac{4g_0^2}{\kappa\gamma_m}$ can be used to calculate the single photon coupling strength giving $g_0 \approx 2\pi\times 0.62$ Hz, close to the value expected from the geometric capacitance. We achieve a maximum multi-photon coupling strength $g \sim 2\pi \times 14$ kHz with $n_d \approx 5 \times 10^8$.

We conclude by discussing future prospects of the graphene microwave optomechanical device we have presented. With the bath temperature of 14 mK, we expect a thermal occupation of our resonator in the range of $\bar{n}_{th} = \frac{k_B T}{\hbar\omega_m} = 8$. With the cooperativity we extract from our measurements, our current experiment is already in the regime $C + 1 > \bar{n}_{th}$, suggesting we should be able to cool to the quantum ground state. We also note that although other experiments have achieved a much larger absolute cooperativity[20], only two optomechanical experiments so far have reached $C + 1 > \bar{n}_{th}$[15,22]. The maximum cooperativity in

present experiment is limited by the maximum power of our signal generator could deliver at the cavity. The superconducting cavity used here can sustain a factor of 5 more photons before it becomes nonlinear, suggesting possible future improvement of C. Furthermore, as $\frac{C}{\bar{n}_{th}}$ is expected to be scale as A^2/t, where A and t are the area and thickness of the resonator respectively, significant improvement can be made by making bigger and thinner resonators. Quantum applications aside, using our graphene optomechanical device, we have demonstrated 17 dB microwave amplification, potential for microwave photon storage for up to 10 ms, and observed a record-high graphene mechanical quality factor $Q_m \sim 220,000$ using radiation pressure force driving. We have also achieved displacement sensitivity of 55 fm/$\sqrt{\text{Hz}}$ with a bandwidth 3 orders of magnitude larger than the mechanical dissipation rate ($\kappa/\gamma_m \sim 10^3$). This provides an unprecedented new tool for studying phenomena as nonlinear restoring forces, nonlinear damping, and mode coupling in graphene. Finally, the simplicity of the microwave design paves the way to study other mechanical resonators from layered materials following this bottom-up approach.

Methods

We have used Mo/Re alloy to fabricate the superconducting cavity. Large superconducting transition temperature ($T_c \sim 8$ K) allows us to achieve large dynamic range of the cavity. To fabricate the quarter wavelength superconducting cavity in coplanar waveguide geometry, we first clean the intrinsic Si substrate with hydrofluoric acid. These substrates were immediately loaded for sputtering and a layer of 300 nm Mo/Re was deposited. Following standard e-beam lithography (EBL) and reactive ion etching procedures, we etched out a quarter wavelength cavity. We follow an additional step of EBL and etching in order to thin down the gate electrode by 150 nm.

---

* Electronic address: g.a.steele@tudelft.nl

[1] Bunch, J. S. *et al.* Electromechanical resonators from graphene sheets. *Science* **315**, 490–493 (2007). PMID: 17255506.

[2] Chen, C. *et al.* Performance of monolayer graphene nanomechanical resonators with electrical readout. *Nat Nano* **4**, 861–867 (2009).

[3] Singh, V. *et al.* Probing thermal expansion of graphene and modal dispersion at low-temperature using graphene nanoelectromechanical systems resonators. *Nanotechnology* **21**, 165204 (2010).

[4] Barton, R. A. *et al.* High, size-dependent quality factor in an array of graphene mechanical resonators. *Nano Letters* **11**, 1232–1236 (2011).

[5] Eichler, A. *et al.* Nonlinear damping in mechanical resonators made from carbon nanotubes and graphene. *Nature Nanotechnology* **6**, 339–342 (2011).

[6] Song, X. *et al.* Stamp transferred suspended graphene mechanical resonators for radio frequency electrical readout. *Nano Letters* **12**, 198–202 (2012).

[7] Barton, R. A. *et al.* Photothermal self-oscillation and laser cooling of graphene optomechanical systems. *Nano Letters* **12**, 4681–4686 (2012).

[8] Chen, C. *et al.* Graphene mechanical oscillators with tunable frequency. *Nature Nanotechnology* **8**, 923–927 (2013).

[9] Regal, C. A., Teufel, J. D. & Lehnert, K. W. Measuring nanomechanical motion with a microwave cavity interferometer. *Nature Physics* **4**, 555–560 (2008).

[10] Teufel, J. D., Donner, T., Castellanos-Beltran, M. A., Harlow, J. W. & Lehnert, K. W. Nanomechanical motion measured with an imprecision below that at the standard quantum limit. *Nature Nanotechnology* **4**, 820–823 (2009).

[11] Rocheleau, T. *et al.* Preparation and detection of a mechanical resonator near the ground state of motion. *Nature* **463**, 72–75 (2010).

[12] Teufel, J. D. *et al.* Circuit cavity electromechanics in the strong-coupling regime. *Nature* **471**, 204–208 (2011).

[13] Massel, F. *et al.* Microwave amplification with nanomechanical resonators. *Nature* **480**, 351–354 (2011).

[14] Hocke, F. *et al.* Electromechanically induced absorption in a circuit nano-electromechanical system. *New Journal of Physics* **14**, 123037 (2012).

[15] Teufel, J. D. *et al.* Sideband cooling of micromechanical motion to the quantum ground state. *Nature* **475**, 359–363 (2011).

[16] Palomaki, T. A., Teufel, J. D., Simmonds, R. W. & Lehnert, K. W. Entangling mechanical motion with microwave fields. *Science* **342**, 710–713 (2013). PMID: 24091706.

[17] Agarwal, G. S. & Huang, S. Electromagnetically induced transparency in mechanical effects of light. *Physical Review A* **81**, 041803 (2010).

[18] Weis, S. *et al.* Optomechanically induced transparency. *Science* **330**, 1520–1523 (2010). PMID: 21071628.

[19] Safavi-Naeini, A. H. *et al.* Electromagnetically induced transparency and slow light with optomechanics. *Nature* **472**, 69–73 (2011).

[20] Gröblacher, S., Hammerer, K., Vanner, M. R. & Aspelmeyer, M. Observation of strong coupling between a micromechanical resonator and an optical cavity field. *Nature* **460**, 724–727 (2009).

[21] Aspelmeyer, M., Kippenberg, T. J. & Marquardt, F. Cavity optomechanics. *arXiv:1303.0733* (2013).

[22] Chan, J. *et al.* Laser cooling of a nanomechanical oscillator into its quantum ground state. *Nature* **478**, 89–92 (2011).

[23] Castellanos-Gomez, A. *et al.* Deterministic transfer of two-dimensional materials by all-dry viscoelastic stamping. *arXiv:1311.4829* (2013).

[24] The motion of graphene capacitor will also modulate the linewidth of the cavity, known as dissipative coupling; proposed recently to enable some novel optomechanical phenomena[26,27]. In our design, the dissipative coupling is significantly weaker than the dispersive coupling and will be neglected. Additional details are provided in the supplementary information.

[25] Zhou, X. *et al.* Slowing, advancing and switching of microwave signals using circuit nanoelectromechanics. *Nature Physics* **9**, 179–184 (2013).

[26] Weiss, T., Bruder, C. & Nunnenkamp, A. Strong-coupling effects in dissipatively coupled optomechanical systems. *New Journal of Physics* **15**, 045017 (2013).

[27] Elste, F., Girvin, S. M. & Clerk, A. A. Quantum noise interference and backaction cooling in cavity nanomechanics. *Physical Review Letters* **102**, 207209 (2009).

Acknowledgments

Authors would like to thank Aashish Clerk for providing initial theoretical input. This work was supported by the Dutch Organization for Fundamental Research on Matter (FOM). A.C.G. acknowledges financial support through the FP7-Marie Curie project PIEF-GA-2011-300802 ('STRENGTHNANO')

Author contributions

V.S., S.B. and B.S. optimized and fabricated the quarter wavelength superconducting cavity (SC) samples. A.C.G. developed the deterministic transfer method. V.S. and A.C.G. transfered graphene on the SC samples. V.S. and S.B. set up the low temperature microwave measurement setup. V.S. performed the measurement. Y.B. provided theoretical support. G.A.S. conceived the experiment and supervised the work. All authors contributed to writing the manuscript and give critical comments.

Additional information

Supplementary information is available in the online version of the paper. Reprints and permissions information is available online at www.nature.com/reprints. Correspondence and requests for materials should be addressed to V.S. or G.A.S.

Competing financial interests

The authors declare no competing financial interests.

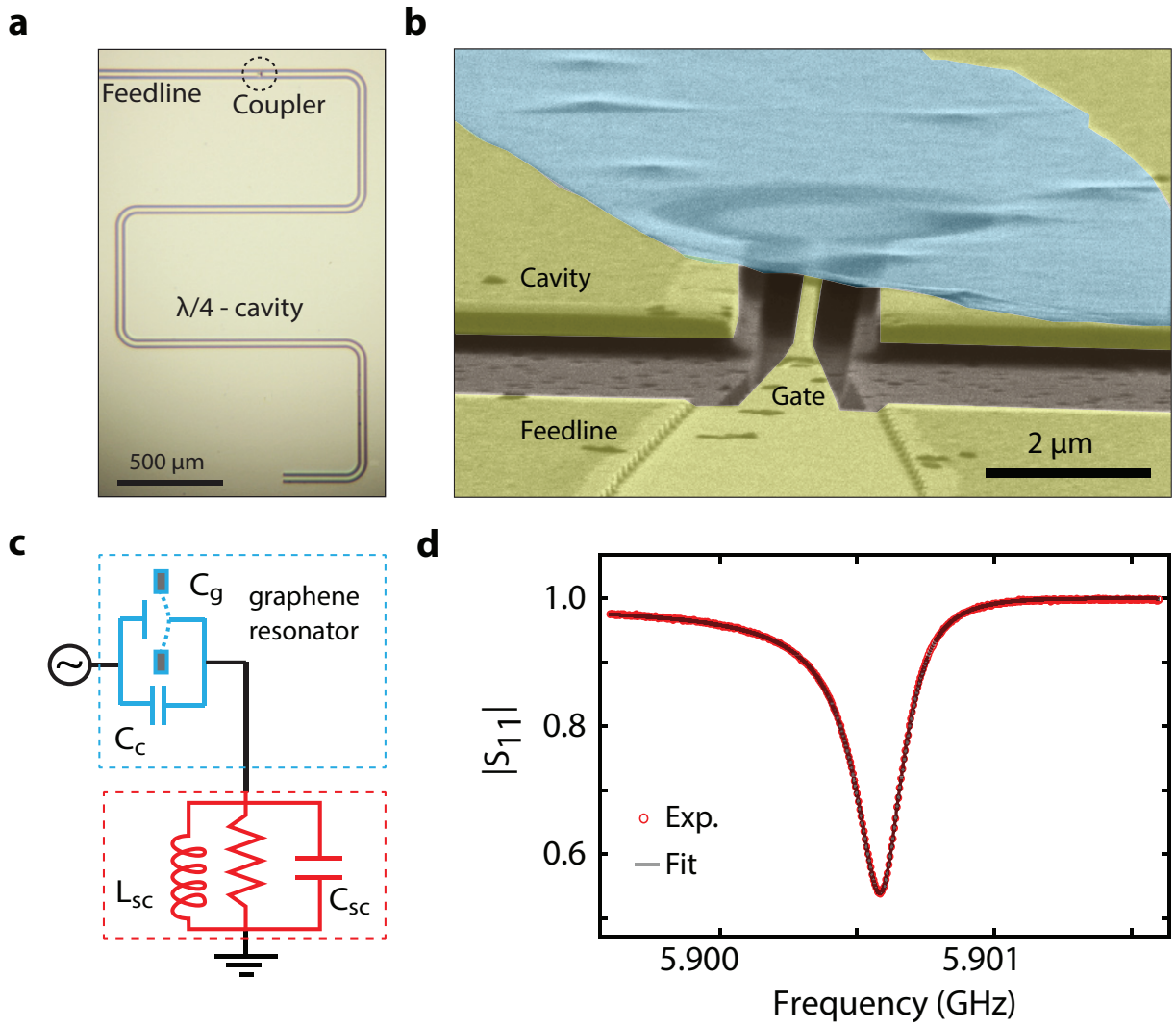

FIG. 1: **Characterization of the superconducting cavity coupled to a graphene mechanical resonator.** (a) Optical image of a superconducting cavity in a quarter wave coplanar waveguide geometry coupled to the feedline with a gap and a gate capacitor (coupler). (b) A tilted angle scanning electron micrograph (false color) near the coupler showing 4 μm diameter multilayer (10 nm thick) graphene resonator (cyan) suspended 150 nm above the gate. (c) Schematic lumped element representation of the device with the equivalent lumped parameters as $C_{sc} \approx$ 415 fF and $L_{sc} \approx 1.75$ nH. (d) Reflection coefficient $|S_{11}|$ of the superconducting cavity measured at $T = 14$ mK (red). Gray curve is a fit to the data, giving the internal quality factor $Q_i \approx 107000$ and loaded quality factor $Q_L \approx 24250$.

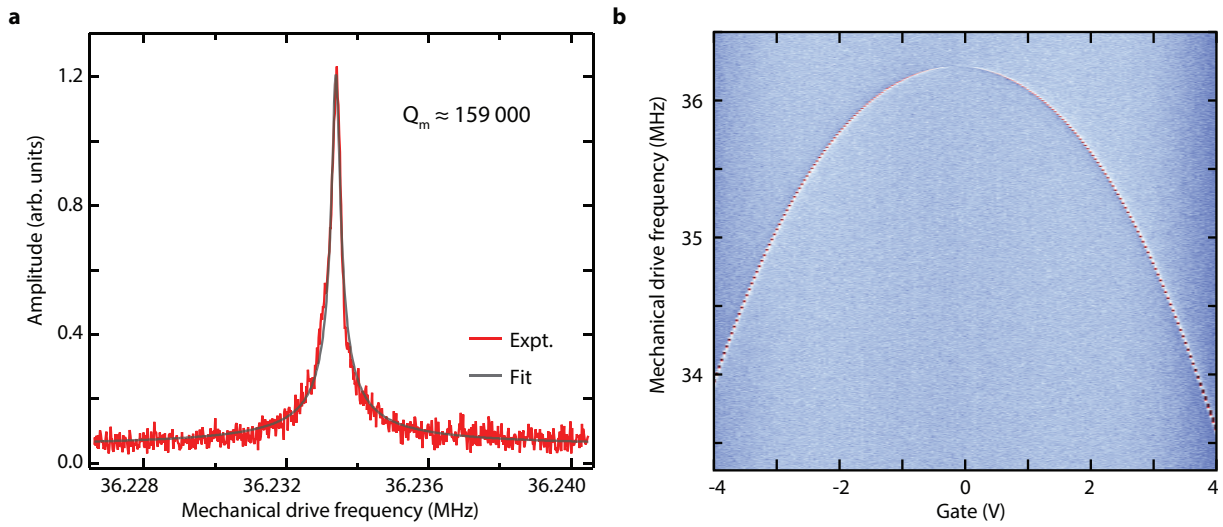

FIG. 2: **Sideband resolved detection of graphene motion.** (a) Driven response of the graphene resonator at $V_g = 150$ mV (red curve). A Lorentzian fit (gray curve) to the response gives the mechanical quality factor $Q_m \approx 159000$, corresponding to mechanical dissipation rate $\gamma_m \approx 2\pi \times 228$ Hz. Mechanical frequency $\omega_m \approx 36.233$ MHz and cavity linewidth $\kappa = 242$ kHz implies a sideband resolved limit ($\omega_m \gg \kappa$). (b) Colorscale plot of the homodyne signal with mechanical drive frequency and gate voltage. The sharp change in color represents the resonance frequency of the graphene resonator, indicating its negative tunability with gate voltage.

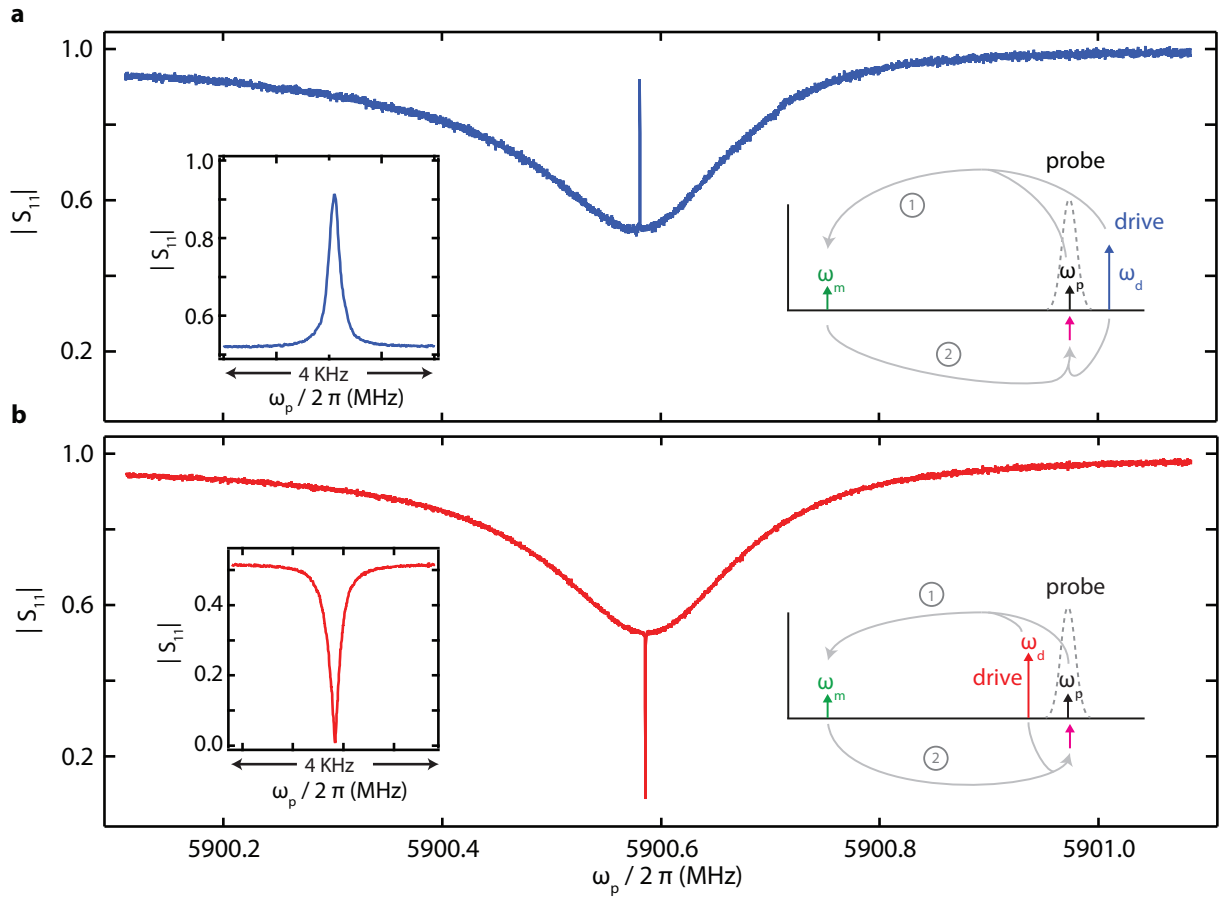

FIG. 3: **Optomechanically induced absorption (OMIA) and reflection (OMIR).** Measurement of the cavity reflection $|S_{11}|$ in presence of sideband detuned drive tone at $V_g = 0$ V. (a) A blue detuned drive results in a window of optomechanically induced reflection (OMIR) in the cavity response. Inset: Zoom of the OMIR window. (b) A red detuned sideband drive opens an optomechanically induced absorption (OMIA) feature in the cavity response. Inset shows zoom of the OMIA. Schematics in (a) and (b) illustrate the OMIR-OMIA features in terms of the interference of the probe field (black arrow) with the microwave photons that are cyclically down and then up converted by the optomechanical interaction (pink arrow).

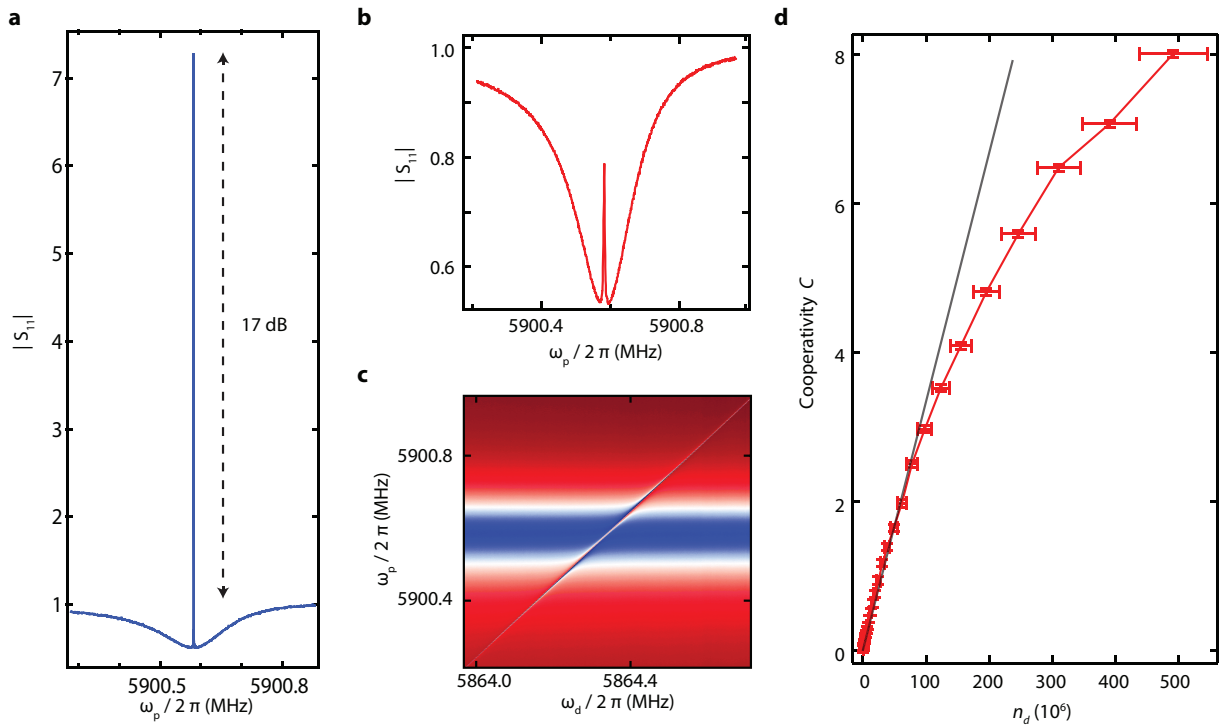

FIG. 4: **Large cooperativity with a graphene mechanical resonator.** (a) Measurement of the cavity reflection $|S_{11}|$ under a strong blue detuned drive ($n_d \approx 10^8$). At the center of the cavity response, the reflection coefficient exceeds 1, corresponding to mechanical microwave amplification of 17 dB by the graphene resonator. (b) Measurement of the cavity reflection $|S_{11}|$ under a strong red detuned drive ($n_d \approx 5 \times 10^8$). With strong red detuned drive, the OMIA feature becomes OMIR and we observe the onset of the normal mode splitting. Also visible in the colorscale plot in (c) as an avoided crossing while sweeping the drive frequency across the red sideband. (d) Plot of cooperativity C vs the number of red detuned photons n_d, where we obtained $C = 8$. The gray line is a linear fit for C for low number of n_d giving single photon coupling strength of $g_0 \approx 2\pi \times 0.62$ Hz. We achieve a maximum multi-photon coupling strength $g \approx 2\pi \times 14$ kHz with $n_d \approx 5 \times 10^8$. The horizontal error bars result from the uncertainty in microwave power reaching at the cavity.

arXiv:1403.5165v1 [cond-mat.mes-hall] 20 Mar 2014

Supplementary Information: Optomechanical coupling between a graphene mechanical resonator and a superconducting microwave cavity

V. Singh, S. J. Bosman, B. H. Schneider,

Y. M. Blanter, A. Castellanos-Gomez and G. A. Steele*

Kavli Institute of NanoScience, Delft University of Technology,

PO Box 5046, 2600 GA, Delft, The Netherlands.

(Dated: March 21, 2014)

S1. COMPARISON BETWEEN DISPERSIVE AND DISSIPATIVE COUPLING STRENGTH :

The dimensionless dispersive $\tilde{A}$ and dissipative $\tilde{B}$ coupling strength are given by[S1],

$$\tilde{A} = \frac{1}{\kappa}\frac{d\omega_c}{dx}x_{zpf} \quad \text{and} \quad \tilde{B} = \frac{1}{\kappa}\frac{d\kappa}{dx}x_{zpf} \tag{S1}$$

where, ω_c is the cavity resonant frequency, κ is total dissipation rate, and x_{zpf} is amplitude of the quantum zero point fluctuations of the mechanical resonator. Utilizing the lumped element model as described in the main text, the ratio between $\tilde{A}$ and $\tilde{B}$ can be written as,

$$\frac{\tilde{B}}{\tilde{A}} \simeq 2\frac{\kappa}{\omega_c}\frac{C_{sc}}{C_e} \tag{S2}$$

where, $C_e = C_g + C_c$ is total coupling capacitance between microwave feedline and superconducting cavity. Using the parameters of the device described in the main text, we obtain $\left(\frac{\tilde{B}}{\tilde{A}}\right)^2 \approx 3 \times 10^{-4}$, which is significantly smaller.

S2. CAVITY CHARACTERIZATION :

The reflection from a single port cavity can be described by[S2],

$$S_{11} = \frac{\frac{\kappa_i - \kappa_e}{2} - i(\omega - \omega_c)}{\frac{\kappa_i + \kappa_e}{2} - i(\omega - \omega_c)} \tag{S3}$$

where κ_i and κ_e are the internal and external dissipation rate of the cavity. It is interesting to note that at the resonant frequency the reflection coefficient $S_{11}^0 = |S_{11}(\omega = \omega_c)| = |1 - 2\frac{\kappa_e}{\kappa}|$ is determined by the coupling efficiency $\eta \equiv \frac{\kappa_e}{\kappa}$. Any small deviation from the ideal Lorentzian response arising from impedance mismatch near the coupler[S3] can be corrected by considering a complex coupling decay rate $\kappa_e = |\kappa_e|e^{i\phi}$.

Figure S1(a) shows the schematic of the complete measurement setup used for cavity characterization. From a vector network analyzer, a microwave signal is sent to the device through highly attenuated cables. A cold circulator is used to measure the reflection from the cavity. Reflected signal is then amplified by a low noise amplifier (LNA) with a noise temperature of $\approx$ 2.7 K. To apply DC gate voltage on the microwave feedline, we use a separate DC line (highly filtered with low pass RC and copper power filter) and a bias tee to add it to the microwave feedline. Figure S1(b) shows the plot of the internal decay rate

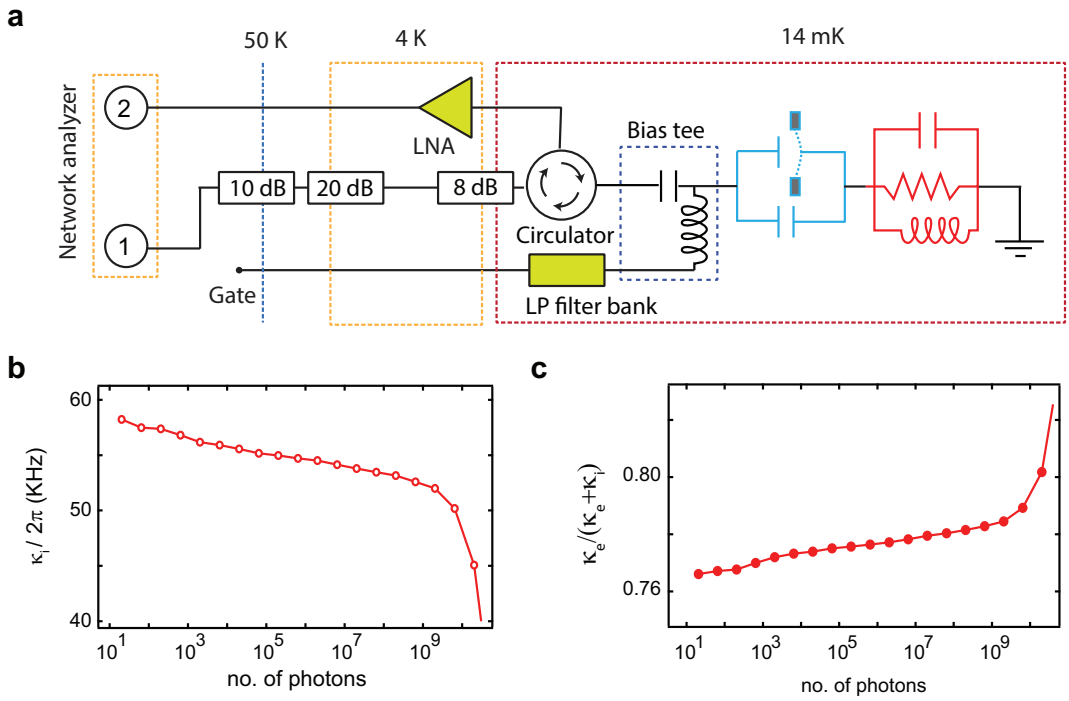

Figure S1: a) Schematic of the complete measurement setup. b) Plot of the internal decay rate κ_i of the cavity with the number of probe photons inside the cavity. c) Plot of coupling fraction $\frac{\kappa_e}{\kappa_e+\kappa_i}$ with number of probe photons inside the cavity.

of the cavity with varied number of probe photons. The presence of the two level systems in the cavity leads to a larger decay rate when probed with small number of photons. As it can be seen from the figure, with large number of the probe photons, internal decay rate reduces, which is a direct consequence of the saturation of the losses due to the two level systems. With further increase in power, kinetic inductance of Mo/Re starts playing a role and κ_i shows a sharper drop eventually turning into a nonlinear response of the cavity. Figure S1(c) shows the plot of coupling efficiency $\eta = \frac{\kappa_e}{\kappa_e+\kappa_i}$ with number of photons. If the number of probe photons becomes large, κ_i reduces and hence enhances the coupling efficiency.

S3. CHARACTERIZATION OF GRAPHENE RESONATOR:

As described in the main text, graphene dynamics is probed with the homodyne measurement scheme, which allows to measure both quadrature of the mechanical motion. In this scheme, the cavity is driven near its resonance frequency ω_c (where the slope of any of

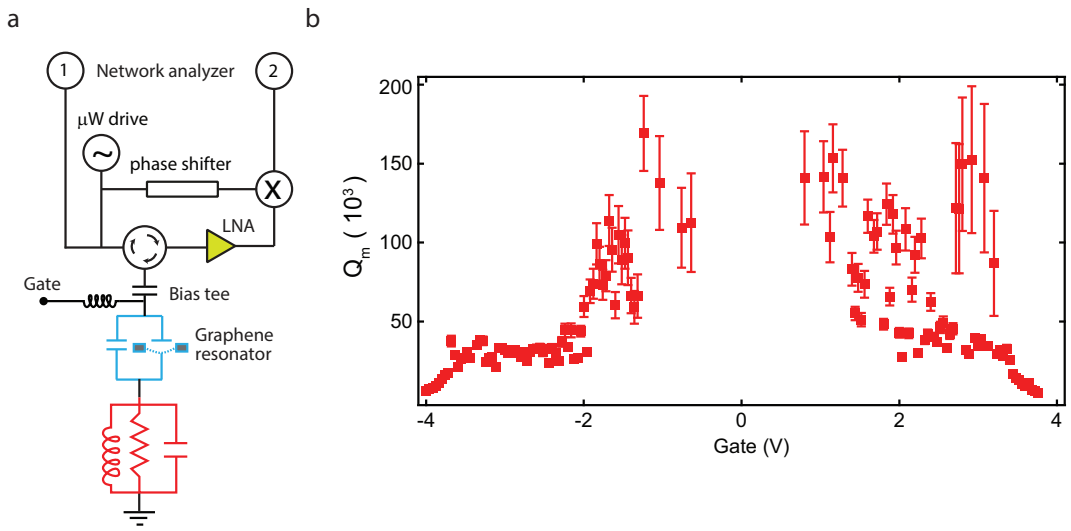

Figure S2: (a) Schematic of the homodyne measurement setup to probe the graphene mechanical resonator. (b) Plot of the mechanical quality factor of the graphene resonator.

the quadrature of the cavity response is maximum). The mechanical resonator is driven by an electrostatic drive (using the source of vector network analyzer) by adding a low power RF signal to the feedline and by applying a DC gate voltage. The mechanical driving force is given by $\frac{dC_g}{dx}V_{ac}V_g$. Near the mechanical resonance, the graphene resonator acquires large amplitude. This motion modulates the microwave signal reflected from the cavity and produces signals at frequency $\omega_c \pm \omega_m$. These sidebands along with the carrier signal are routed towards a low noise amplifier using a circulator. At room temperature, we demodulate this signal by mixing it with the phase adjusted carrier reference. The demodulated signal is filtered, amplified and fed into the second port of the vector network analyzer. A measurement of S_{21} in this setup directly probes the responsivity of the mechanical resonator. Using $S_{21} \propto \omega_m^2/(\omega_m^2 - \omega^2 + i\omega\omega_m/Q_m)$, mechanical resonant frequency ω_m and quality factor Q_m can be extracted. Figure S2(b) shows the plot of mechanical quality factor with gate voltage, extracted from the data shown in Figure 2(b) of the main text.

S4. OPTOMECHANICAL INTERACTION :

S4.1. Optomechanical induced absorption and reflection

To explain the optomechanical effects on the cavity, we have followed the approach taken in the supporting online material of ref [S4]. Our starting point is the expression for the field amplitude A^- inside the cavity at the probe frequency given by

$$A^- = -\sqrt{\kappa_e} S_p \frac{1 + if(\Omega)}{i(\bar{\Delta} + \Omega) - \kappa/2 - 2\bar{\Delta} f(\Omega)}, \tag{S4}$$

where

$$f(\Omega) = \hbar G^2 \bar{a}^2 \frac{\chi(\Omega)}{i(\bar{\Delta} - \Omega) + \kappa/2} \tag{S5}$$

and

$$\chi(\Omega) = \frac{1}{m_{eff}} \frac{1}{\omega_m^2 - \Omega^2 - i\Omega\gamma_m}. \tag{S6}$$

Here κ_e is the external decay rate, κ is total cavity decay rate, S_p is the probe amplitude, G is the cavity pull-in factor, $\bar{a}$ is the drive field amplitude, $\Omega = \omega_p - \omega_d$ is the beating frequency, $\bar{\Delta} = \omega_d - \omega_c$ is the detuning of the drive signal from the cavity center frequency, ω_m is the resonance frequency of the mechanical resonator, m_{eff} is the effective mass of the resonator, and γ_m is mechanical dissipation rate.

To relate A^- to the reflection coefficient of the cavity, we use the input-output relation for a single port cavity, defining

$$S_{11} = 1 - \sqrt{\kappa_e} \frac{A^-}{S_p}. \tag{S7}$$

For a **red** detuned drive, we take $\bar{\Delta} = -\omega_m$ and $\Omega \simeq \omega_m$. We introduce $\Delta' = \Omega - \omega_m$ as a small detuning parameter. Taking a resolved sideband approximation $\kappa \ll \omega_m$, we get

$$\chi(\Omega) = -\frac{1}{2m_{eff}\omega_m} \frac{1}{\Delta' + i\gamma_m/2} \tag{S8}$$

and

$$f(\Omega) = -\frac{ig^2}{8\omega_m} \frac{1}{\Delta' + i\gamma_m/2} \tag{S9}$$

where we have used $g = G\bar{a}\sqrt{\frac{\hbar}{2m_{eff}\omega_m}}$.

For a **blue** detuned drive, we take $\bar{\Delta} = \omega_m$ and $\Omega \simeq \omega_m$, introducing $\Delta^{'} = \Omega + \omega_m$ as a small detuning parameter. This gives

$$\chi(\Omega) = -\frac{1}{2m_{eff}\omega_m}\frac{1}{\Delta' + i\gamma_m/2} \tag{S10}$$

and

$$f(\Omega) = -\frac{ig^2}{8\omega_m}\frac{1}{\Delta' + i\gamma_m/2}. \tag{S11}$$

By introducing normalized variables, $\eta = \frac{\kappa_e}{\kappa}$, $g^{'} = \frac{g}{\kappa}$,$\gamma = \frac{\gamma_m}{\kappa}$, $\omega = \frac{\omega_p - (\omega_d \pm \omega_m)}{\kappa}$ and $\delta = \frac{\omega_c - (\omega_d \pm \omega_m)}{\kappa}$ the reflection coefficient of the cavity can be written in the following form

$$S_{11}(\omega, \delta) = 1 - \frac{i\eta(-2i\gamma - 4\omega)}{\pm 4g'^2 + (-i + 2\delta - 2\omega)(i\gamma + 2\omega)} \tag{S12}$$

where positive (negative) sign is taken for red (blue) detuned drives.

Backaction on the cavity within the mechanical bandwidth

In the limit of exact detuning, following equation (S12), the magnitude of the cavity reflection at $\omega_p = \omega_c$ can be written as

$$|S_{11}(\omega = 0, \delta = 0)| = \left| 1 - 2\frac{\kappa_e}{\kappa_e + (\kappa_i \pm \frac{4g^2}{\gamma_m})} \right|. \tag{S13}$$

Comparing it with the reflection coefficient of the cavity in absence of the optomechanical coupling *i.e.* $|S_{11}(\omega_p = \omega_c)| = \left|1 - 2\frac{\kappa_e}{\kappa_e + \kappa_i}\right|$, it becomes quite evident that within the mechanical bandwidth the effect of the optomechanical coupling can be captured by modifying internal dissipation rate to $\kappa_i \pm \frac{4g^2}{\gamma_m}$.

S4.2. Measurement of the mechanical quality factor and estimation of the group delay at $V_g = 0$ V

Figure S3(a) shows the schematic of the measurement setup used to study the optomechanical interactions. A weak probe signal is applied using a vector network analyzer. A

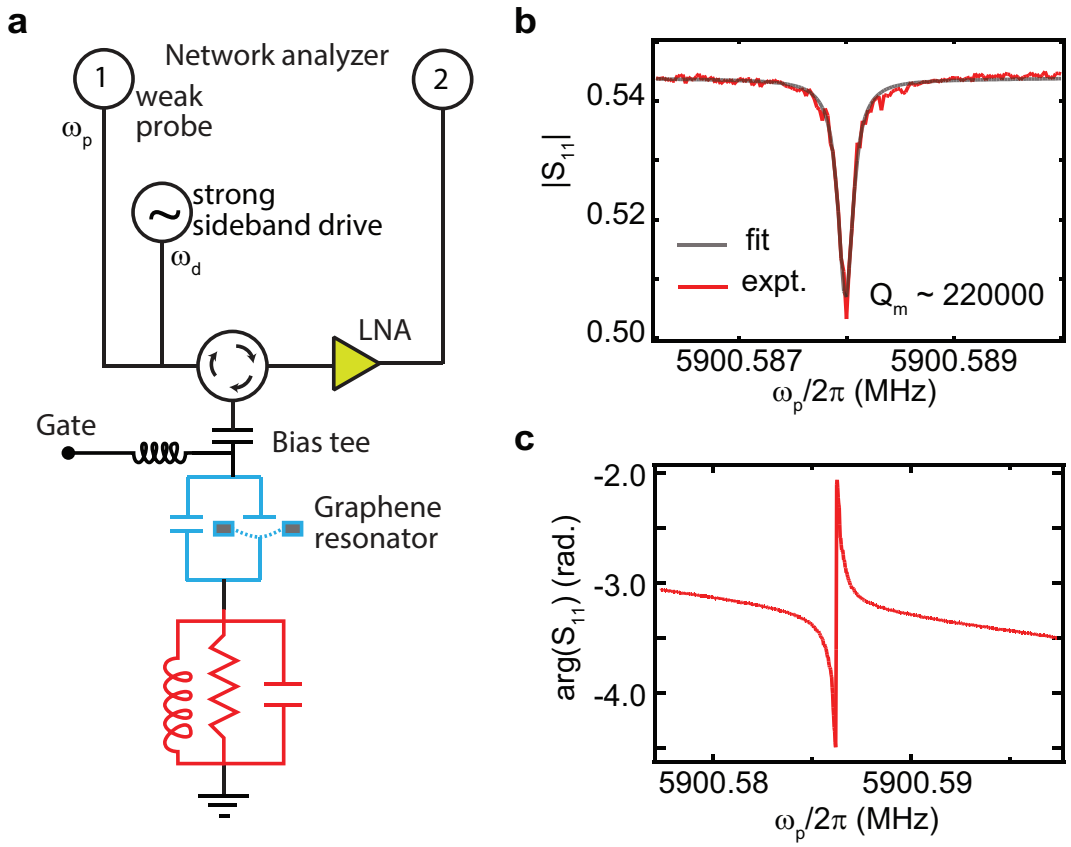

Figure S3: (a) Measurement scheme to probe optomechanical interaction. (b) Detailed measurement of OMIA feature measured with low optomechanical coupling strength (red) along with the fitted curve (gray). (c) Plot of phase of the reflection coefficient measured with red detuned drive. The phase swing in the mechanical bandwidth corresponds to a group delay of ≈10 ms.

separate microwave source is used to drive the cavity near the sidebands. The two signal tones are added using a directional coupler (10 dB). Figure S3(b) shows the measurement of $|S_{11}|$ with small optomechanical coupling strength such that any backaction effect on the mechanical resonator can be ignored (red curve). This can be fit to equation (S12) to yield a mechanical quality factor $Q_m \approx 220{,}000$ at V_g=0 V. Figure S3(c) shows the phase response ϕ of the cavity at somewhat larger coupling strength such that $\kappa_e \simeq \kappa_i + \frac{4g^2}{\gamma_m}$. The swing in the phase can be associated with a group delay $\tau = \frac{\delta\phi}{\delta\Omega}$ of the photons which lie within the mechanical bandwidth at ω_c. From this measurement, we estimated a maximum group delay of $\approx$ 10 ms.

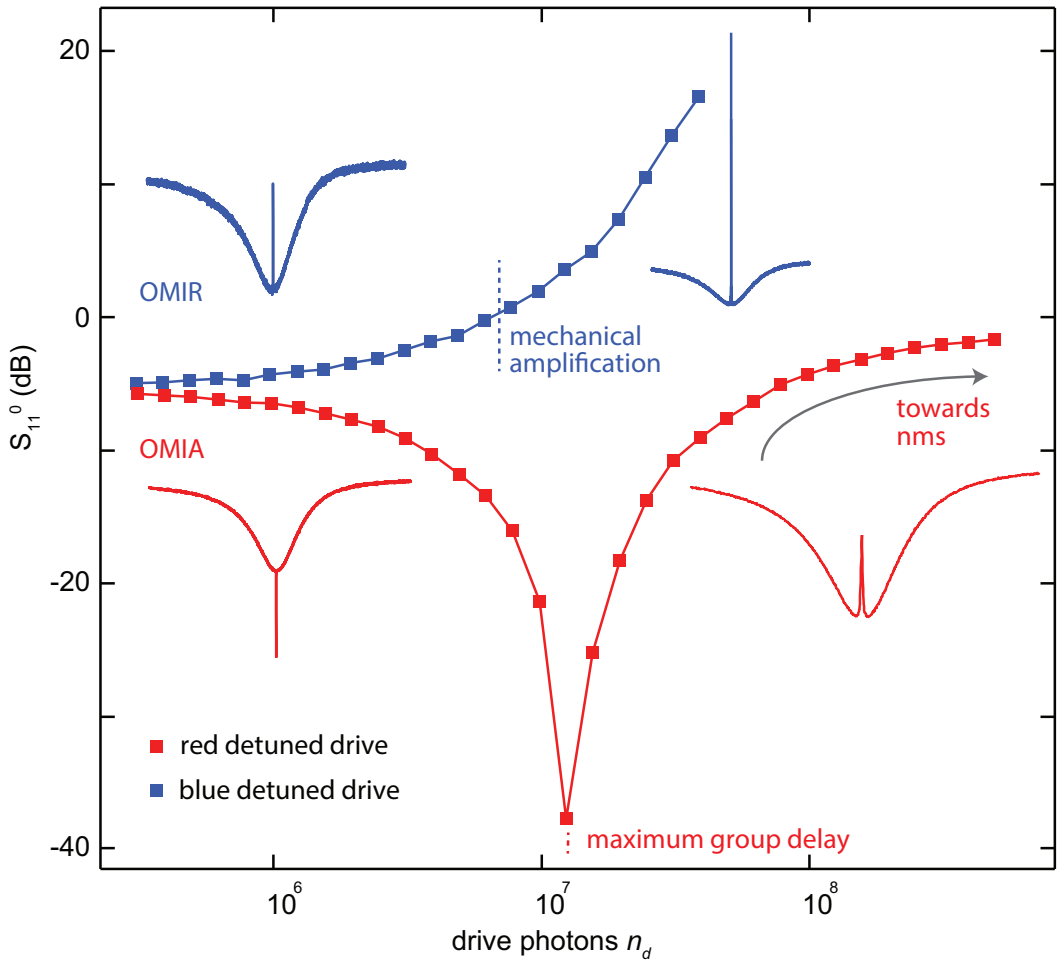

Figure S4: Plot of the reflection coefficient measured at cavity resonance frequency with zero detuning $S_{11}^0 \equiv S_{11}(\omega = 0, \delta = 0)$ of the red and blue detuned drive. Regions with different effects have been marked.

S5. ESTIMATION OF THE COOPERATIVITY :

Using the notion of the optomechanical cooperativity $C = \frac{4g^2}{\kappa\gamma_m}$, equation (S13) can be written as,

$$S_{11}^0 \equiv |S_{11}(\omega = 0, \delta = 0)| = \left|1 - \frac{2\eta}{1 \pm C}\right| \tag{S14}$$

allowing a direct estimation of cooperativity without any free parameters, where positive (negative) sign is taken for red (blue) detuned drive.

Figure S4 shows the plot of $|S_{11}^0|$ with the number of drive photons for the red and blue detuned drives. For a blue detuned drive while increasing the coupling strength (increase

in the number of drive photons), the optomechanical induced reflection (OMIR) feature converts into mechanical amplification ($S_{11}^0(dB) > 0$). This cross over occurs when internal losses in the cavity are balanced by $4g^2/\gamma_m$. For a red detuned drive with increase in the coupling, the optomechanical induced absorption first becomes deeper and then starts to convert into OMIR like feature. This cross over occurs when external losses are balanced by $\kappa_i + 4g^2/\gamma_m$. Any further increase in coupling leads the system towards normal mode splitting (nms) of the cavity resonance (strong coupling limit). Following this measurement, we can estimate the cooperativity C by using equation (S14). The result has been shown in the Figure 4(d) of the main text.

---

* Electronic address: g.a.steele@tudelft.nl

[S1] Elste, F., Girvin, S. M. & Clerk, A. A. Quantum noise interference and backaction cooling in cavity nanomechanics. *Physical Review Letters* **102**, 207209 (2009).

[S2] Aspelmeyer, M., Kippenberg, T. J. & Marquardt, F. Cavity optomechanics. *arXiv:1303.0733* (2013).

[S3] Paik, H. & Osborn, K. D. Reducing quantum-regime dielectric loss of silicon nitride for superconducting quantum circuits. *Applied Physics Letters* **96**, 072505 (2010).

[S4] Weis, S. *et al.* Optomechanically induced transparency. *Science* **330**, 1520–1523 (2010). PMID: 21071628.